Topics in Catalysis (2025) 68:1910–1923
https://doi.org/10.1007/s11244-025-02123-x

ORIGINAL PAPER

Reproducibility of Electrochemical Measurements with Ionic Liquids: Role of Supplied Batches, Water and Adventitious Oxygen

Maren-Kathrin Heubach[1,4] · Fabian M. Schuett[1] · Jerome Mayer[1] · Omar W. Elkhafif[1] · Albert K. Engstfeld[1] · Timo Jacob[1,2,3]

Accepted: 24 May 2025 / Published online: 12 September 2025
© The Author(s) 2025

Abstract

Studying the potential dependent interaction of non-aqueous electrolytes, such as ionic liquids (ILs), with model electrode surfaces plays a crucial role not only in the field of battery-related research. These electrolytes bear the advantage that their electrochemical stability windows often exceed that of water. However, comparing results using ILs as electrolytes reported in the literature reveals strong discrepancies in the reproducibility of the data. In this study, we show that parameters such as the supplier, the supplied batch, and the purification steps can have a huge impact on the electrochemical properties. As a reference system, these properties are studied by cyclic voltammetry on a Au(111) single crystal electrode in *N*-methyl-*N*-propylpiperidinium bis(trifluoromethane)sulfonimide ([MPPip][TFSI]). Analysing the different features observed in the cyclic voltammograms, we were to some extent able to deconvolute the features that are related to the interaction of ILs with the substrate and impurities added from the pretreatment due to the influence of residual water and oxygen.

Graphical Abstract

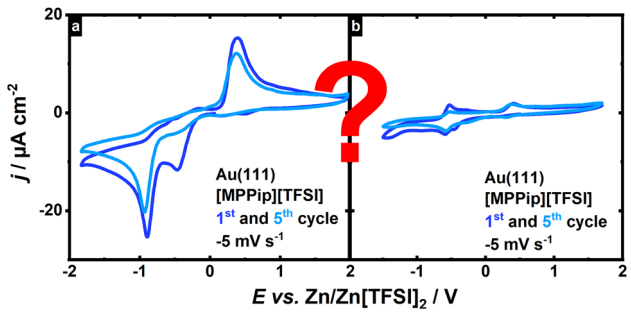

Keywords Ionic liquids · Model electrodes · Gold · Electrochemistry · Reproducibility

✉ Albert K. Engstfeld
albert.engstfeld@uni-ulm.de

✉ Timo Jacob
timo.jacob@uni-ulm.de

[1] Institute of Electrochemistry, Ulm University, D-89081 Ulm, Germany

[2] Helmholtz-Institute-Ulm (HIU) Electrochemical Energy Storage, Helmholtzstr. 11, 89081 Ulm, Germany

[3] Karlsruhe Institute of Technology (KIT), P.O. Box 3640, 76021 Karlsruhe, Germany

[4] Present address: Department of Chemistry, Queen's University, 90 Bader Lane, Ontario K7L 3N6 Kingston, Canada

1 Introduction

In recent years, non-aqueous electrolytes received increasing interest for their application in the area of energy conversion and storage. While in aqueous electrolytes the hydrogen evolution reaction (HER) and the oxygen evolution reaction (OER) usually limit the stability regime of the electrolyte, non-aqueous electrolytes allow studying processes beyond these potential limits [1, 2]. Among the non-aqueous electrolytes, ionic liquids (ILs) are promising candidates due to their high electrochemical and thermal stability [3, 4]. Furthermore, they are intrinsically ion-conducting and have low vapour pressures in contrast to other organic electrolytes considered for such kind of applications [5, 6].

To understand an electrocatalytic reaction, detailed knowledge of the surface redox processes with the supporting electrolyte is indispensable since the components from the electrolyte adsorbed on the surface or found in the electrolyte near the electrode can have a significant influence on the observed activity [7–10]. Preferably, such studies are performed on well-defined single crystal electrodes, acting as a benchmark and allowing for direct comparison between theory and experiment, as shown for example for Au(111) [11–13], Cu(100) [14, 15], or Ag(111) [16, 17]. A prominent model electrode is Au(111) since Au is rather inert and different preparation procedures yield reproducible clean surfaces [18].

Cyclic voltammetry is well-suited to study the potential dependent interaction of ILs with different substrates. The features observed within their electrochemical stability window can be attributed to a variety of processes, such as adsorption [19, 20] or reductive decomposition of anions [21, 22]. These electrochemical features can overlap with those induced by impurities, such as residual halide and alkali metal ions, originating from the IL synthesis [23], residual oxygen [7, 24, 25], or residual water [26, 27], or a combination of both [28, 29]. Interestingly, it was observed that current–voltage transients of an IL can be nearly featureless within the electrochemical stability window if the experiment is performed under vacuum conditions or in a purified Ar atmosphere [24].

Studying the influence of residual water in ILs is an important aspect since water has a tremendous impact on electrocatalytic reactions [30], such as the oxygen reduction reaction (ORR) [27], or metal deposition [31, 32]. Additionally, residual water can lead to unwanted side reactions or a decrease of the electrochemical stability window of the IL [30, 33–35]. The uptake of water depends on the particular IL and occurs in contact with water or even the surrounding atmosphere. It has been shown that this is the case for both hydrophilic and hydrophobic ILs [1, 36].

Thus, in order to improve the reproducibility of the obtained system behaviour when using ILs as electrolytes, purification steps that reduce the amount of water, oxygen and other volatile compounds seem mandatory. This can, for example, be achieved by a combination of heat and vacuum treatments [28, 37–39]. Another purification method involves binding of the impurities to a solid phase such as activated carbon [40] or a molecular sieve [31, 41, 42]. Molecular sieves are made of zeolites and their pore dimensions determine their selectivity in removing certain types of differently-sized impurities [43]. For instance, detailed studies revealed that molecular sieves of 3−4 Å pore size are well-suited for removing water [30, 31, 41]. However, even if molecular sieves are thought to be rather clean and able to remove water from the ILs, it should be noted that they might also introduce new unwanted impurities by ion exchange into the IL [44].

Overall, the electrochemical behaviour of a certain IL on a specific electrode material is often hard to reproduce since the synthesis and purification of these chemicals is rather tedious. For example, it has been shown that even different batches of an IL can behave differently, as illustrated by a set of cyclic voltammograms (CVs) extracted from the literature in Fig. 1 [45–48]. All CVs show the electrochemical behaviour of *N*-butyl-*N*-methylpyrrolidinium bis(trifluoromethane)sulfonimide ([BMPyr][TFSI]) on a Au(111) electrode. For comparison, the different curves were adjusted to a specific peak, which is explained in more detail in the data evaluation section of the SI. Fig. 1d) shows two curves from the same publication, but with different potential limits. A similar behaviour is observed by comparing CVs recorded in [MPPip][TFSI] from the same supplier on Au(111) published by our group within the last five years (see SI Figure S1) [39, 49].

To understand these differences in more detail, in this work, we revisited the electrochemical properties of the very same electrolyte used previously ([MPPip][TFSI]) on Au(111), where both the IL and the electrode have been subject to extensive studies at our institute, thus allowing also a good comparison with these former studies. Due to its broad electrochemical stability window, this electrolyte was also used in former studies related to metal deposition [39, 49, 51]. Using cyclic voltammetry, we systematically studied the electrochemical behaviour of different batches of the same IL, purchased on different dates from different suppliers. Hereby, the well-defined Au(111) single crystal serves as a probe to determine the quality of the IL. For unambiguous interpretation of the data, all measurements were conducted in the potential region where the electrode is stable, i.e., no irreversible structrual changes are observed. In particular, we explored how the CVs changed by varying the lower potential limit and after recording multiple potential

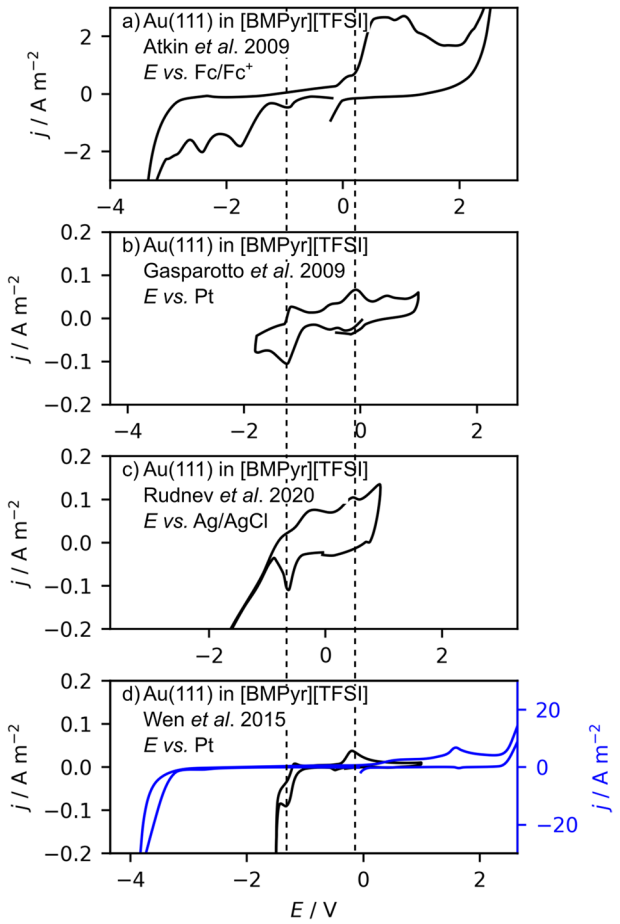

Fig. 1 Different published CVs for Au(111) recorded in [BMPyr][TFSI] with 10 mVs^{-1}. All CVs were digitized, using the Python module svgdigitizer [50]. The curves were extracted from the work of (**a**) Atkin et al. [45], (**b**) Gasparotto et al. [46], (**c**) Rudnev et al. [47], and (**d**) Wen et al. [48].

Table 1 Summary of the supplier (1–Iolitec, 2–Solvionic), date of purchase, and purity of the different batches.

ID	Supplier	Purchased	Purity (%)
Batch 1	1	11.2017	99
Batch 2	1	09.2020	99
Batch 3	1	05.2021	99
Batch 4	2	06.2021	99.9
Batch 5	1	08.2022	99

Measurements with batch 5 are only shown in the SI. Information about the halide content and the synthesis (provided by the supplier) is given in the SI (Table S1)

cycles with the same potential limits. Similar experiments were performed with ILs pretreated in different ways, i.e., drying the IL in a vacuum and at elevated temperatures, adding molecular sieves after this procedure, or by increasing the water content, which inevitably also introduces trace amounts of oxygen. The role of other possible contaminants originating from the manufacturing process or from the addition of the molecular sieve is discussed as well.

2 Experimental

2.1 Materials

Five separate batches of the IL [MPPip][TFSI] were purchased from two suppliers with a stated purity of either 99% or 99.9%. Details about the origin, purity, and purchase date are given in Table 1. Ultrapure water (18.2 MΩcm) from a *Sartorius Arium Pro* water system was used for cleaning the electrochemical equipment. The water added to the ILs was also taken from this system. The working electrode consists of a Au(111) single crystal with a diameter of 12 mm purchased from *MaTecK*.

2.2 Electrolyte Preparation

Batches 3, 4 and 5 were used as received, without any further purification steps unless explicitly specified. In contrast, batches 1 and 2 were always vacuum-dried. The drying process of the ILs under vacuum were done with a rotary vane pump at the minimal pressure of 10^{-3} mbar and 60 °C overnight, while stirring the electrolyte. In some experiments, a molecular sieve (4 Å, Merck) was added to the IL prior to the purification with vacuum and heat treatment, as described before. Details about the water content and preparation procedure of each measurement are summarised in Tables S2–3 of the SI. The ILs were prepared in an *MBRAUN LABStar* glove box with a N_2 (5.0, *MTI IndustrieGase AG*) atmosphere (O_2 and H_2O content $\leq$ 0.5 ppm).Only the addition of water was done under atmospheric conditions. After water addition, the vial with the IL was exposed to vacuum with a rotary vane pump at the minimal pressure of 10^{-3} mbar for 3–5 cycles of approximately 30 s and consecutive flushed with N_2 (5.0, *MTI IndustrieGase AG*) to deaerate the electrolyte. All water contents were determined by Karl-Fischer-titration using a Karl-Fischer coulometer *851 Titrando* by *Metrohm*.

2.3 Sample Preparation

The disc-shaped Au(111) single crystal (*MaTecK*, 12 mm diameter) was annealed in air in a muffle furnace (*Carbolite CWF 1200*) for at least 2 h at 960 °C before each experiment and cooled in air, which was shown to yield clean and flat electrode surfaces [39, 51].

2.4 Electrochemical Setup

All electrochemical measurements were carried out in an *MBRAUN LABStar* glove box with a N_2 (5.0, *MTI IndustrieGase AG*) atmosphere (O_2 and H_2O content $\leq$ 0.5 ppm). A home-built electrochemical cell made from Kel–F and

designed for small amounts of electrolyte was used. The cell was sealed with an O-ring on the electrode, whose inner diameter of $1.1\mathrm{cm}^2$ defined the available electrochemical active surface area. A Zn wire (5N, *MaTecK*) being in contact with a saturated solution of $\mathrm{Zn[TFSI]_2}$ (99.5%, *Solvionic*) in [MPPip][TFSI] (99%, *IoLiTec*) served as a homemade reference electrode. A detailed description of the preparation of such electrodes and their long-time stability can be found in Ref [52]. The reference electrode has an electrode potential of −0.65 V *vs.* the $\mathrm{Fc/Fc^+}$ redox-couple and the shift in the potential is lower than 23 mV $\mathrm{h^{-1}}$. A Pt wire (99.99%, *MaTecK*) was used as counter electrode. The potentials of the electrodes were controlled with a *Zahner IM6* potentiostat operated with the *Thales Z* software.

3 Results

First, the general electrochemical behaviour of the different batches of [MPPip][TFSI] in contact with a Au(111) single crystal will be discussed, illustrating the dependence of the observed cyclic voltammetry peaks on the applied potential limits. Next, the influence of the different pretreatments as well as the water content, will be shown. Note that, in this manuscript, we mainly show results for the IL denoted as batch 3. Similar trends were also observed for the other batches, which are indicated in the text and are depicted accordingly in the supporting information. The trends shown in this study are representative for several measurements that were performed in the same way. Comparing the individual measurements showed negligible variations in the observed features. Note that all cyclic voltammetry measurements shown in this study were performed in a potential window in which the Au electrode does not undergo irreversible restructuring of the surface. Thus, all changes observed in the voltammetric traces should be related to the interaction of the electrode with the electrolyte and possible changes of the electrolyte.

3.1 Dependence on Batch Number

The electrochemical properties of Au(111) in four different batches of the same IL (see Table 1) were studied by cyclic voltammetry. For each measurement, the first CV is shown in Fig. 2, where the starting potential was always set to 0.5 V, scanning to negative potentials first, with a scan rate of 5 mV $\mathrm{s^{-1}}$. The lower and upper potential limits (LPL and UPL) were set to −1.5 V and 1.7 V. All potentials in this work were referenced *versus* the $\mathrm{Zn/Zn[TFSI]_2}$ redox-couple. Consecutive potential cycles lead to subtle

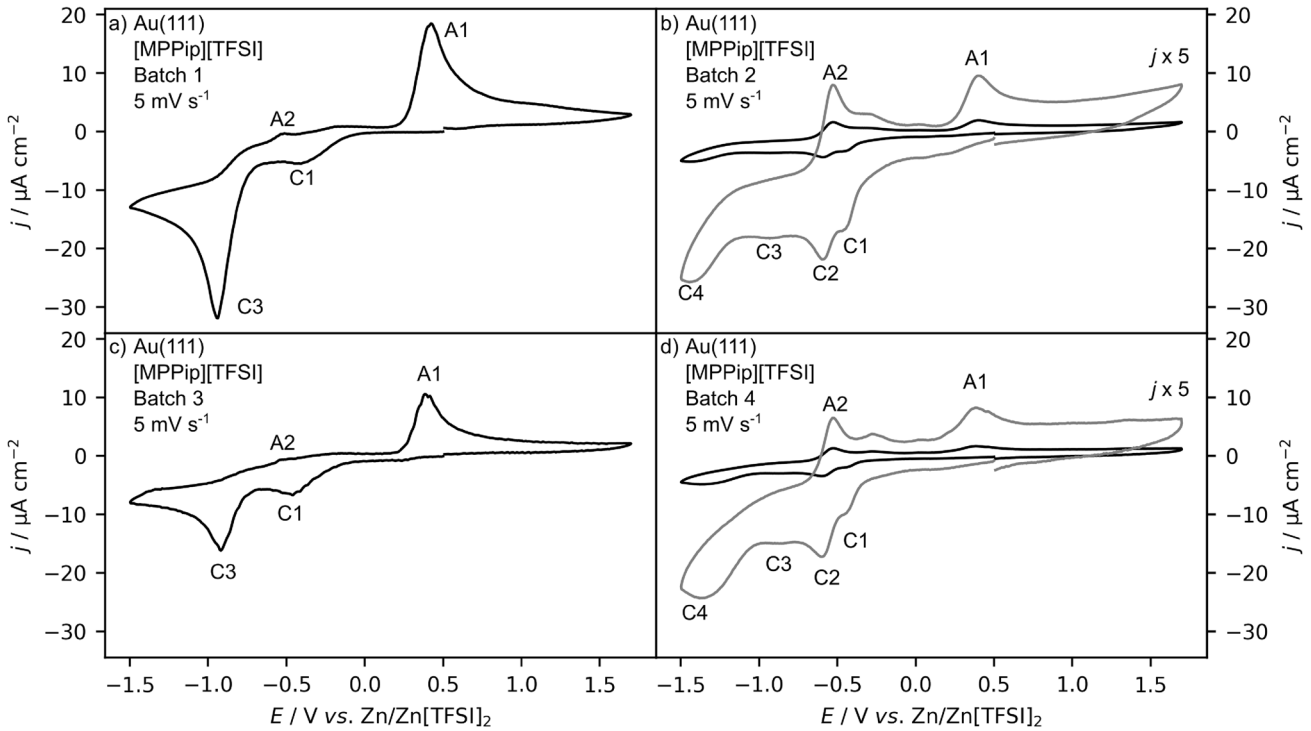

Fig. 2 CVs for Au(111) recorded in different batches of [MPPip][TFSI]. In each case, the first potential cycle is shown. Additional potential cycles can be found in Figure S2 in the SI. The CVs were recorded at a scan rate of 5 mV $\mathrm{s^{-1}}$. The starting potential was set to 0.5 V, scanning to negative potentials first. Grey curves show the current density scaled by a factor of five. For details on the peaks and the categorisation of batches 1 (**a**) and 3 (**c**) into the electrochemical behaviour of type I and batches 2 (**b**) and 4 (**d**) of type II, we refer to the text.

changes in some peaks of the CVs, as illustrated in Figure S2, showing the first and fifth potential cycles. The key peaks described below can be resolved in all potential cycles. In addition, the cathodic current density decreases with increasing number of potential cycles.

Comparing the first potential cycles recorded with the different batches reveals significant differences in the electrochemical behaviour of the individual batches. Nevertheless, the behaviour of batches 1 and 3 (Fig. 2a, c), as well as that of batches 2 and 4 (Fig. 2b, d), are rather similar and are henceforth denoted as type I (left column) and type II (right column), respectively.

Specifically, the CVs for type I show three distinct peaks, i.e., in the negative-going scan peaks C1 (−0.45 V) and C3 (−0.9 V), and in the positive-going scan peak A1 (0.4 V). In some measurements, an additional less pronounced peak A2 is observed at −0.5 V in the positive-going scan. In the case of type II, the current density in the CVs is much lower compared to that in the CVs with type I. For better comparison and visibility of the features, a rescaled CV (factor five) is shown as a grey curve in Fig. 2b, d. In the CVs with type II, additional peaks can be observed in the negative-going scan direction, i.e., peaks C2 (−0.6 V) and C4 (−1.4 V). In the positive-going scan, peak A2 (−0.5 V) is more pronounced and observed in every measurement. The peaks C1 and A1 from type I are still clearly visible, even though the current density of the peaks is about five times lower. The intensity of peak C3 from type I is also much lower and it is not well resolved.

To distinguish between surface redox processes and possible electrocatalytic reactions, we determined the total charge passed in both scan directions for regions with positive and negative current densities. The corresponding values for batches 3 and 4 (from Fig. 2c, d) are summarized in Table 2. Considering that one electron is transferred per surface atom and that a reconstructed Au(111) surface consists of 1.4×10^{15} atoms per cm^2, one would expect a charge of 222 $\mu C\,cm^{-2}$. However, a single molecule from the IL is larger than a Au atom on the surface and hence covers several sites. Consequently, the total charge for monolayer adsorption is lower compared to the case where adsorbates cover every single surface atom.

In type I, the total charge passed in regions with negative current density exceeds the charge of 222 $\mu C\,cm^{-2}$ significantly. In the case of type II, the total charge passed is lower compared to that of type I, but still larger than that for a single electron transfer per surface atom. The charges are also higher than that expected for a process involving two electrons, such as the formation of an atomic oxygen layer by water dissociation. Larger charges could indicate bulk or near-surface oxidation, which would lead to significant electrode restructuring during continuous potential cycling. This process is, however, rather unlikely on Au(111) under these conditions. Thus, for both types, an electrocatalytic process is expected to occur concomitantly with the surface redox processes, which will be discussed below.

Comparing the batch supplier and stated purity of the ILs (see Table 1), with the results shown in Fig. 2, we find that the electrochemical behaviour of both types can be observed (i) with batches supplied from a single supplier and (ii) independent from the stated purity. Hence, neither the purity nor the supplier is considered to be at the origin of the different behaviours observed in Fig. 2. Nevertheless, it is very interesting that the electrochemical behaviour of all investigated batches can be categorized into these two distinct types.

Table 2 Total charge passed in regions with negative current densities (cathodic) and positive current densities (anodic) in the first potential cycle of type I in Fig. 2c (batch 3) and type II in Fig. 2d (batch 4).

	Type	Charge/μC cm^{-2}
Type I	Cathodic	−3060
Type I	Anodic	1260
Type II	Cathodic	−1200
Type II	Anodic	505

3.2 Impact of the LPL

To correlate the peaks in the negative-going scan with those in the positive-going scan for both types (batches 3 and 4 in Fig. 2), we recorded a series of CVs in a set of window opening experiments, where the UPL was fixed at 1.7 V and the LPL was decreased from 0.0 V (grey) to −0.5 V (blue), −1.0 V (red), and −1.5 V (black), as illustrated in Fig. 3. The first potential cycle between 0.0 V and 1.7 V is denoted as initial CV. Note that for this initial CV the potential was scanned in the positive direction, while for all other CVs, the potential was scanned to negative potentials with respect to the starting potential. In this potential window, the scan direction barely has an influence. For each potential window, two consecutive CVs were recorded, of which only the first is shown. The second potential cycles in comparison to the first for each potential window are shown in Figure S3. In addition, after decreasing the LPL and recording two potential cycles, the LPL was again set to 0.0 V (the potential window of the initial CV), recording a minimum of two potential cycles until the deviations from the initial CV become insignificant. The corresponding CVs in the potential window of the initial CV are shown in Figure S4b. Since the initial CVs look almost identical after each experimental step, we infer that the initial composition of the electrolyte in the region close to the electrode can be restored after the excursion to lower potential limits. However, in some cases, several potential cycles are needed to

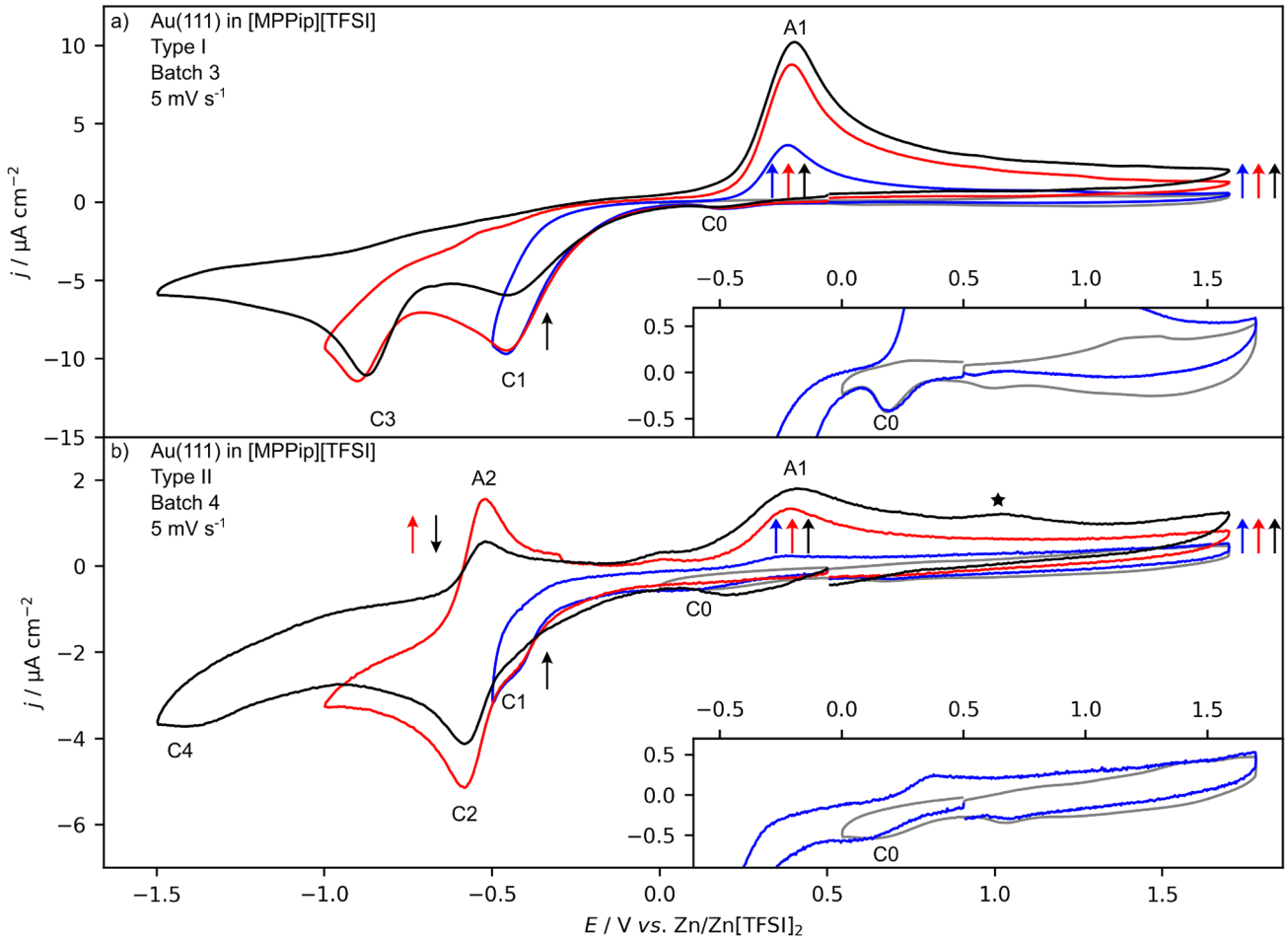

Fig. 3 CVs for Au(111) recorded in [MPPip][TFSI] of both types shown in Fig. 2, with (**a**) batch 3 and (**b**) batch 4. The LPL was decreased from 0.0 V (grey) to −0.5 V (blue), −1.0 V (red), and −1.5 V (black) while the UPL was constantly set at 1.7 V. The insets show a magnification of the low current region of the CV recorded with a LPL of 0.0 V. For clarity, only the first of two CVs, recorded with the respective LPL, are shown. The coloured arrows indicate which features increase or decrease with each lowering of the LPL.

restore the initial behaviour, indicating that this process is determined by kinetics and/or diffusion within this region.

A detailed description of the wide range of large and subtle changes in CVs occurring with different LPLs can be found in the SI. The most important aspects are the following:

(i) The positive-going scan of both types does not show any significant features as long as the LPL is not exceeding 0.0 V.

(ii) peak A1 appears once the LPL is extended into peak C1 and increases further by lowering the LPL beyond peak C1. Simultaneously, the current density increases for potentials more positive than that of peak A1. The CVs within the initial potential window of 0.0 V to 1.7 V, recorded in-between, still show a small hump at the position of peak A1 which decreases during consecutive potential cycles. Likewise, the current density at potentials positive of peak A1 decreases with every potential cycle and approximates to its initial value. The lower the LPL, the more potential cycles are required in the initial potential range to revert the CV to its initial state.

(iii) peak C1 decreases with every subsequent potential cycle when the LPL is below −0.5 V.

(iv) With a LPL of −1.5 V, in the CVs that show type II a broad feature appears at potentials positive of peak A1 in the positive-going scan (indicated by a star symbol in Fig. 3). Additionally, it was observed that the current density in the peak pair C2/A2 in type II (Fig. 3b) decreases with every potential cycle.

Despite the differences between type I and II, most trends of the window opening experiment are observed in both cases.

3.3 Influence of Water

3.3.1 Water Removal

To reduce the water content, the ILs were usually pretreated by vacuum-drying and/or the addition of a molecular sieve [26, 31]. Other contaminants could be metal or halide impurities originating from the manufacturing process or the pretreatment [23]. Thus, in this section we focus on the influence of small amounts of water, studying the effects of different water amounts on the electrochemical properties of the system.

The batches of the IL presented in this study were, according to the supplier and confirmed by our Karl-Fischer measurements, delivered with a water content in the range of 5–100 ppm (see Table S1–2 in the SI). In this section, we illustrate the effect of reducing the water content for batch 3 (type I). This batch had an initial water content of 100 ppm, which was (i) reduced to 20–50 ppm in different measurements, by drying the IL in vacuum (10^{-3} mbar) at 80 °C overnight ($t \geq 12$ h) or (ii) reduced to less than 5 ppm by addition of a 4 Å molecular sieve prior to treating the IL with the procedure in (i). Figure 4 shows a comparison of the CVs obtained by both purification methods (solid lines) in a and b, compared to the measurements performed with the as-received IL (dashed lines). The experimental procedure was identical to that presented in Fig. 3, where the LPL was gradually decreased. The data for both pretreatments indicate that the removal of water has only minor effects on the different peaks. All peaks remain at the same potential. After the pretreatment with heat and vacuum, only peak C1 decreases to some extent. Nevertheless, this effect is small. Previous reports showed that in some cases this treatment even leads to an increase in all observed peaks [31]. Pretreating the IL in addition with a molecular sieve, leads in all measurements to an overall decrease of peak A1, for all investigated lower potential limits. Decreasing the LPL to even more negative values after the treatment with a molecular sieve, results in more significant changes in both scan directions for batches 3 and 4, as shown in the supporting information in Figure S6–7.

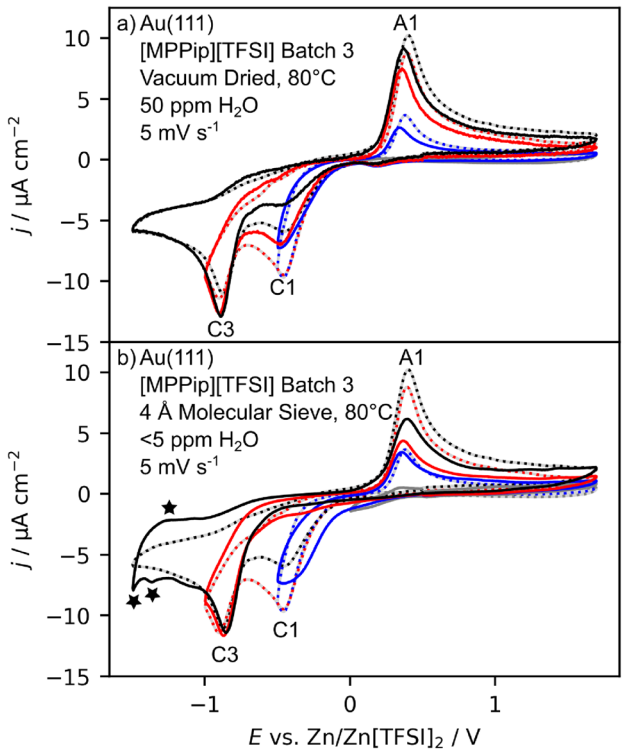

Fig. 4 CVs for Au(111) recorded in [MPPip][TFSI] (batch 3– type I) at a scan rate of 5 mV s^{-1}, where the IL was pretreated (**a**) by drying in vacuum overnight (50 ppm residual H_2O), or (**b**) by drying at vacuum overnight after addition of a 4 Å molecular sieve(<5 ppm residual H_2O). The LPL was gradually decreased from 0.0 V to −0.5 V, −1.0 V, and −1.5 V. The UPL was kept constant at 1.7 V. A more detailed description of the experimental procedure can be found in the text to Fig. 3. Each CV represents the first potential cycle recorded within the respective potential windows. The dotted lines show the same experiment with the same batch without any purification steps (shown in Fig. 3).

It should also be mentioned that after the molecular sieve treatment, two small peaks in the negative-going scan (−1.4 V, −1.5 V) and one in the positive-going scan (−1.3 V) appear (marked by stars in Fig. 4b). Since the positions of these peaks are rather similar to those observed in measurements where Na was explicitly deposited from the same IL (type I) on a Au(111) surface [51], these might indeed be related to Na, whose origin could be multi-fold, including possible ion exchange of Na from the molecular sieve with cations of the IL. A similar effect has been reported previously, however, for an IL in contact with a molecular sieve at elevated temperatures [44]. On the other hand, in an experiment where Na[TFSI] was added with a concentration of 5 mM, not all of the here-reported peaks (especially those at potentials larger than 0.5 V) were observed and it was concluded that Na is not responsible for the newly observed features after the treatment of the IL with a molecular sieve [31]. In addition, these Na impurities might interact with the trace amounts of water in the systems, an aspect that would require further investigations. Finally, the addition of a molecular sieve to batches showing type II also has a significant impact on the electrochemical properties, as illustrated in the SI (Fig. S7). In that case, the peak-pair C2/A2 disappears almost completely, while the other features that are apparent in the CV recorded in the IL without any pretreatment does not change significantly. Possible reasons for the change in C2/A2 are discussed below.

3.3.2 Water Addition

Next, we discuss the effect of adding water to the as-received IL on the electrochemical properties. Here, approximately 150–200 ppm water was added to batches 3 and 4, resulting in total water contents of 270 ppm and 170 ppm, respectively. The 1st (black solid line) and 5th CV (red solid line) are shown in Fig. 5. The CVs for the as-received batches (without additional water) are shown for comparison (dotted lines).

Although there are obvious issues of adding water to the hydrophobic ionic liquid, some distinct changes could be observed. For type I, especially in the first potential cycle, peak C1 is significantly larger when adding water to the system, while peak C3 is almost not visible. After several potential cycles, the current density of peak C1 decreased but is still larger than that in the as-received electrolyte. Peak C3 in turn emerges as an individual feature in consecutive potential cycles.

For type II, the peaks C2, C4 and A2 increased with water addition. Additionally, the current density positive of peak A1 is higher and some broad peaks become visible in this potential range. In the following potential cycles, the peaks C2 and C4 decrease, but the current densities are still higher compared to those recorded in the as-received ILs. The size of peak A2 also decreases, and its size is almost identical to that in the CV for the as-received IL after five potential cycles.

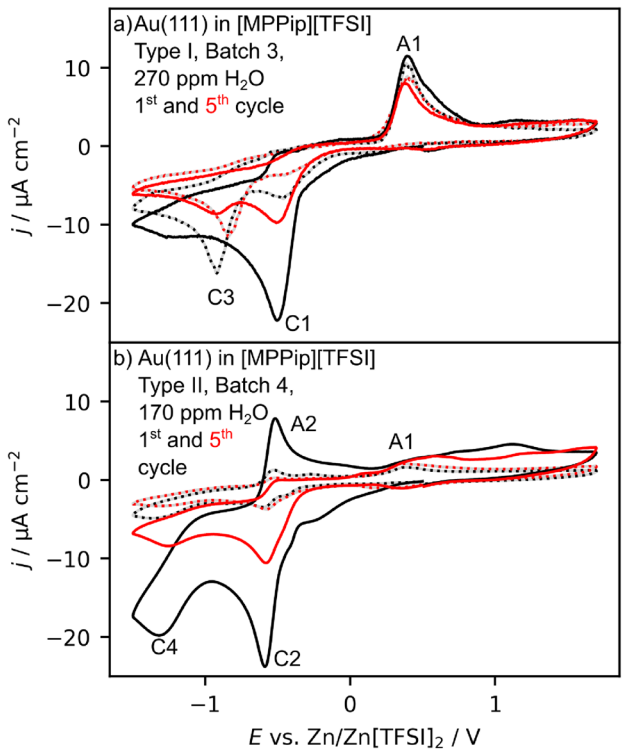

Fig. 5 CVs for Au(111) in [MPPip][TFSI] of (**a**) batch 3 and (**b**) batch 4 with approx. 150 ppm water added. The 1st potential cycle of each experiment is shown in black and the 5th potential cycle in red. The dashed lines show the CVs for the corresponding batches without additional water.

Comparing both types, it is apparent that the processes of peaks C1 and C2 occur at similar potentials. Since the peaks are only separated by ca. 0.1 V, and hence overlap, the actual size of the individual peaks can not be inferred. We assume that peak C2 in batch 4 (Fig. 5b) is indeed a combination of the processes related to peaks C1 and C2. First, we have shown above, that peak C2 is related to peak A2 in the positive-going scan, and thus peak A2 will possibly only increase when peak C2 increases. Second, a similar experiment performed with batch 2 (see Figure S7a in the SI) also shows a peak pair C2/A2 in the CV without additional water. Upon the addition of water, the current density of both peaks C1 and C2 increases in this case, where peak C2 is clearly separated from peak C1. Based on these results we are confident that the intensity of both peaks C1 and C2 increases with the addition of water to the IL.

Figure 6 shows the evolution of the CV for Au(111) in the IL with a water content of 450 ppm (higher content than in the previous experiment), recorded after different times of storage of the IL in the glove box (from 12 h to five days). Note that each of these measurements was performed in a freshly prepared cell with electrolyte freshly taken at the respective time from the same container, which was stored in the glovebox. With Karl-Fischer titration, we found that the water content in the stored IL was constant over the investigated time. First, by comparing the CVs measured here (having 450 ppm water) with those containing 270 ppm water (Fig. 5), we did not observe a significant increase of peak C1. On the contrary, the peak is smaller than in the measurement with 270 ppm water. This could already show a first effect of storage time since the measurement in Fig. 5 was recorded directly after adding the water to the IL. The most notable observation is that peak C1 decreases with increasing storage time, while peak C3 increases. After five days, the CV looks almost identical to the CV recorded in the as-received IL with a water content of less than 75 ppm.

3.4 Discussion

Based on our results, we identified two different electrochemical behaviours for [MPPip][TFSI] on Au(111), reflected by different peaks and current densities in different potential regions. In the following, the role and possible type of impurities are discussed, primarily focusing on the influence of water and the impurities introduced in the system by its removal or addition.

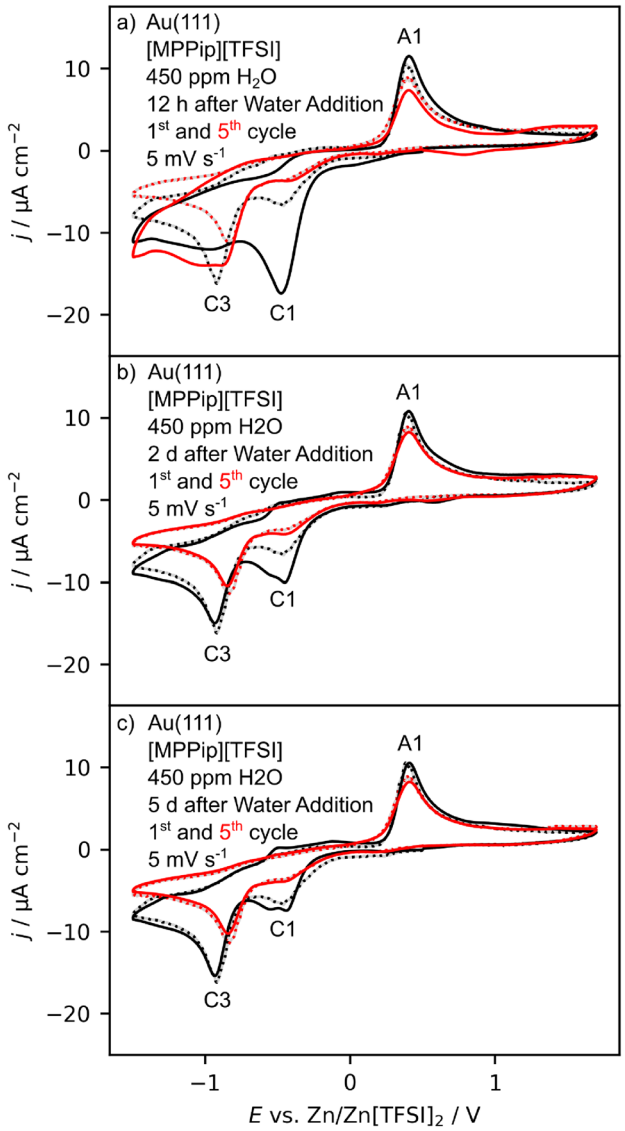

Fig. 6 Effect of storage time after water addition in air on the CV for Au(111) in [MPPip][TFSI] of batch 3 with 450 ppm water. The CVs were recorded (**a**) 12 h, (**b**) 2 d, and (**c**) 5 d after the water addition. Note that all measurements were performed in a freshly prepared cell with fresh electrolyte taken from an IL stored for the denoted amount of time in the glove box. The dotted lines indicate the same measurement without water addition and the scan rate was 5 mV s^{-1}.

3.4.1 Batch Differences

From studying five batches of the same IL ([MPPip][TFSI]) from two suppliers and different purchase dates, we observed two distinctly different electrochemical behaviours in the CVs recorded on Au(111). This result does not rule out that other batches from the same or even other suppliers might behave differently. We suggest that impurities are at the origin of the observed differences, which can contribute in different ways to the electrochemical behaviour of the system. First, the impurities themselves can adsorb on the surface, thus taking part in the adlayer formation on the surface, which can result in additional peaks in the CV (when the process involves a charge transfer process). Secondly, the impurities could also be continuously converted catalytically, which results in a current that adds to the currents related to the surface redox process of adlayer formation. We assume that a combination of both effects takes place on the electrode surface, since (i) we observe different peaks in both behaviours and (ii) based on our evaluation of the charges passed in regions with negative or positive currents, it is clear that the observed current densities are not only related to surface ad- and desorption processes (the total charges exceed those of monolayer adsorbate layer formation).

In general, the most common impurities are residual atmospheric oxygen and water [26, 28]. Other possible contaminants that remain in the IL from the synthesis are metal and halide ions, or organic solvents [23, 53–55]. Metal ion contamination can lead to additional features in a CV, which are related to their deposition and/or dissolution [23]. Following, we will thus discuss the role of different types of impurities.

Whether or not trace metals are present in the IL, which can be deposited on the surface, can for example be studied by *in-situ* scanning tunnelling microscopy (STM), which allows depicting structural changes of the surface upon their deposition [23]. In a former *in-situ* STM study using the same batches of as-received ILs used in the present work, we could not find evidence of metal deposition [51].

The presence of residual halides has been shown to decrease the stability of the IL at high positive potentials at the anode [54, 56]. For the ILs used in this work the suppliers stated a halide content below 100 ppm for all batches. We did not verify the stability of the ILs at high decomposition potentials, to elucidate a possible difference in halide content in the different batches. Thus, its impact still remains unknown in our case. Additionally, the IL could contain different organic impurities as well as residues from the reactants and byproducts in the ionic liquid's synthesis, which could equally influence the electrochemical behaviour.

Considering that the ILs contain different impurities, one can derive the following conclusions to rationalise the differences between type I and II. (i) The peaks C1, C3 and A1 observed in type I are related to an impurity which is present in a higher concentration in the batches with type I than in batches of type II. The presence of these species could block the surface for other processes, such as those observed with type II in peaks C2/A2 and C4. (ii) Likewise, an impurity inducing the processes related to peaks C2 and C4 could block the surface for the processes related to peaks C1, C3, and A1.

3.4.2 Influence of Water

The role of water on the electrochemical properties of an IL in contact with an electrode, in general, has been studied previously [26, 27, 30, 33–35]. These studies often focus on the distribution of water at the solid 33, 34] and on the electrochemical stability window of the IL [27, 35]. A few of the latter studies did show the emergence of features similar to peaks C1 or C3 in type I observed in the present work [26, 29]. To address the influence of water, we briefly comment on the different water sources in such measurements and how they would impact the overall behaviour. A less commonly addressed origin is the native water film that develops on an electrode surface following its preparation, typically occurring during the transfer of the electrode to the electrochemical cell, often located within a glove box [41]. In this case, the amount of water on the surface should be rather similar for all experiments. Assuming that the water reacts on the substrate when a potential is applied, the related current response should possibly be small and only be visible within the first potential cycle. This phenomenon could, at least to some extent, rationalise the observed changes of the CV within the first potential cycles in our experiments (see Figure S2).

However, commonly water is already present in the as-received ILs, and thus has to be removed carefully [57, 58]. Approaches to reduce the amount of water in the ILs used in the present work have been suggested previously, which involve drying and heating in vacuum, followed by treating the IL with a molecular sieve [31, 41]. Our results indicate that using heating and vacuum alone on the herein studied IL, has no significant impact on the electrochemical properties, even though the water content decreases. Regarding the addition of a molecular sieve, there exist contradictory conclusions on the most suitable pore size (3 Å [41] *vs*. 4 Å [31] – used in this work and Ref. 31). We assume that the ability to remove water also depends on the batch and supplier of the molecular sieve. Our measurements revealed additional peaks in the CVs when a molecular sieve was involved in the drying process. Specifically, we assume that these peaks are related to Na, based on the positions of the peaks in the CV, which are similar to those noted during Na deposition on Au(111) from the same IL in a previous work [51]. Additional XPS measurements confirmed the presence of Na in the IL [59], whose origin might be related to various sources.

Reducing the amount of water in the IL has no significant effect on the electrochemical properties. In contrast, water addition led to an increase of the cathodic peaks C1 for type I and peaks C2 and C4 for type II (see Fig. 5) (though we speculated that peak C1 overlaps with peak C2 in type II). We found that independent of the amount of water added (100 ppm to 400 ppm), the first potential cycles showed a very similar behaviour. However, storing the IL in a glove box for several hours or even days, leads to a gradual decrease of peak C1 of type I (see Fig. 6) even though the water content remained unchanged. Therefore, peak C1 must be induced by another species that appeared in the IL along with water. A likely candidate is O_2 since the water added to the IL was not deaerated beforehand. We assume that in the glove box, O_2 will gradually be released from the IL. With an IL containing 400 ppm water, this process took two to five days. A big difference was already observed after 12 h. In general, it was suggested that the overall solubility of O_2 and other hardly polarisable gases in ILs is rather low, [60–62] which favours the diffusion of O_2 from the electrolyte into the glovebox. The solubility of O_2 can, however, change in the presence of other species, which was, for example, shown for the co-solvation with CO_2 in [HMIm][TFSI] (1-hexyl-3-methylimidazolium bis(trifluoromethane)sulfonimide) [63]. Further measurements would be required to gain more fundamental insights into such co-solvation effects.

The time-dependence on the IL storage, is an important result as it indicates that the reproducibility of the electrochemical measurements strongly depend on how fast the experiments are performed or how long the chemicals are stored in the glove box before use (to be in equilibrium with the glove box atmosphere). A more detailed possible role of O_2 on the CV will be discussed below.

Finally, note that even though the water itself might not have a measurable impact on the CV recorded in the as-received IL, it has been shown to play an important role in other processes. Examples are metal deposition [31, 32] or electrocatalytic reactions, such as the oxidation of organic molecules [30], and the ORR [27].

3.4.3 Residual Oxygen

To understand the role of residual oxygen in our measurements, we briefly describe the key aspects of the ORR in ILs on various substrates [7, 25, 64, 65]. Different reaction pathways are proposed in the literature [24, 29, 66]. We consider the following pathway for ORR in an initially neutral environment where O_2 is reduced to form a super-oxide radical in a first electron transfer step (Eq. 1) and a peroxide ion in a second electron transfer step (Eq. 2) [24, 25, 66].

$$O_2 + e^- \longrightarrow O_2^{-*} \tag{1}$$

$$O_2^{-*} + e^- \longrightarrow O_2^{2-} \tag{2}$$

In the presence of water, O_2 supposedly reacts with H_2O to form H_2O_2 and/or hydroxide ions (Eqs. 3, 4, 5, 6) [25, 29].

$$O_2 + 2H_2O + 2e^- \longrightarrow H_2O_2 + 2OH^- \quad (3)$$

$$O_2 + 2H_2O + 4e^- \longrightarrow 4OH^- \quad (4)$$

$$O_2 + H_2O + e^- \longrightarrow HO_2^* + OH^- \quad (5)$$

$$2HO_2^* \longrightarrow O_2 + H_2O_2 \quad (6)$$

For the interpretation of our results, we suggest that the reaction of residual O_2 with H_2O is the dominant reaction pathway. Depending on the batch of electrolytes, these processes occur for type I in peak C1 and for type II in peaks C1 and C2. According to Katayama et al. [25], possible products formed within these peaks are reoxidized in the subsequent positive-going scan for type I in peak A1 and for type II in peaks A2 and A1. Considering that the catalytic reaction (no charge transfer) in Eq. 6 (suggested by Katayama et al.) takes place, it is expected that the reduction peaks are larger than the oxidation peaks. This is indeed the case in our experiments and is apparent by the high charge passed in the cathodic current regime compared to the anodic current regime (see Table 2). Interestingly, the size of peak A1 in the positive-going scan decreases only slightly, while peak C1 in the negative-going scan decreases significantly when O_2 is consumed during continuous potential cycling or removed over time from the electrolyte. Thus, the peak must be related to a specific reaction. We suggest that peak A1 is related to the oxidation of OH^-. To verify this assumption, we recorded CVs in [MPPip][TFSI] (type I, batch 3) containing 0.4 M H[TFSI], which is shown in the SI (Figure S8). The addition of H[TFSI] significantly reduces the size of peak A1, which is possibly caused by a decrease of the OH^- concentration due to the recombination with the H^+ ions. Another explanation is the reaction of H^+ ions with O_2 to form hydrogen peroxide as proposed by Switzer et al. and Yuan et al. and given in Eq. 7 [65, 66]. This reaction contributes to the charge during the negative-going scan, but since no OH^- is formed, the charge in peak A1 is smaller.

$$O_2 + 2H^+ + 2e^- \longrightarrow H_2O_2 \quad (7)$$

The peak C3 observed in type I and peak C4 in type II could be related to the reduction of water to form H_2 (Eq. 8) [28, 67].

$$2H_2O + 2e^- \longrightarrow H_2 + 2OH^- \quad (8)$$

This reaction leads to the formation of additional OH^-. The OH^- in turn will be oxidised in peak A1 in the positive-going scan, which indeed leads to an increase of that peak (see Fig. 3).

In total, we suggest that the cathodic peaks, which change over time with consecutive potential cycling or the time an electrolyte is stored in the glove box, result from different contents of residual water and oxygen in the IL. The fact that we observe different peaks, both in the negative and positive going scan in different batches of the same IL, is most likely related to different types of impurities remaining in the IL from the manufacturing process. Whether or not the impurity adsorbs on the surface or changes the local structure of the IL in the double-layer region above the electrode cannot be inferred from our data. Nevertheless, it seems to play an essential role in the potential region where the reduction of residual O_2 in the presence of water takes place and presumably also in the type of product which forms under these circumstances.

4 Conclusion

In this work, we studied the electrochemical properties of different batches of [MPPip][TFSI] with Au(111) in a potential region where the Au(111) electrode did not restructure irreversibly. It was shown that the reproducibility of the results strongly depends on the manufacturer, purchase date and pretreatment of the IL. We were able to categorise the ILs into two distinctly different electrochemical behaviours, which are likely a result of specific types of still unknown impurities. It seems that one of the impurities can be removed to some extent by a molecular sieve. However, this procedure also seems to introduce Na (with the herein-used molecular sieve) as another impurity in the system. In contrast to the common understanding, water, which is discussed to be a native impurity in ILs, does not seem to have a significant impact on the electrochemical properties. The changes observed upon the addition of water were attributed to residual O_2, which has been introduced into the system along with the water. The unknown impurities, in turn, have an impact on the potential region where water and O_2 are catalytically converted. The magnitude of the currents for these conversion reactions possibly strongly depends on the water/O_2 ratio. An important aspect is also that it takes quite some time for O_2 to be released from the IL in the glove box, and hence, the reproducibility also strongly depends on the time of preparation and measurement. We only showed results for one specific IL. However, it can be expected that similar phenomena can be observed for other ILs as well as in other complex electrolytes. In total, our work illustrates the complexity of studying the redox properties of ILs, especially with well-defined electrodes, which are, however, mandatory to derive a clearer picture of interfacial processes.

Acknowledgements This work was funded by the Deutsche Forschungsgemeinschaft (DFG, German Research Foundation) under Germany's Excellence Strategy - EXC 2154 - Project number 390874152. Further, the authors gratefully acknowledge funding by the DFG through project 50180537 as well as by the BMBF (Bundesministerium fur Bildung und Forschung) through the project CASINO (FKZ: 03XP0487G) and the state of Baden-Württemberg and the DFG through grant no INST 40/574-1 FUGG.

Author Contributions M.-K. Heubach: Conceptualisation, Data Curation, Formal Analysis, Investigation, Visualisation, Writing– Original Draft Preparation. F. M. Schuett: Conceptualisation, Writing– Review and Editing. J. Mayer: Data Curation. O. W. Elkhafif: Investigation, Writing– Review and Editing. A. K. Engstfeld: Conceptualisation, Supervision, Writing– Review and Editing. T. Jacob: Resources, Supervision, Writing– Review and Editing.

Funding Open Access funding enabled and organized by Projekt DEAL.

Data Availability The data supporting this study's findings are openly available in Zenodo at http://doi.org/10.5281/zenodo.13123468.

Declarations

Conflict of interest The authors declare no conflict of interest.

Open Access This article is licensed under a Creative Commons Attribution 4.0 International License, which permits use, sharing, adaptation, distribution and reproduction in any medium or format, as long as you give appropriate credit to the original author(s) and the source, provide a link to the Creative Commons licence, and indicate if changes were made. The images or other third party material in this article are included in the article's Creative Commons licence, unless indicated otherwise in a credit line to the material. If material is not included in the article's Creative Commons licence and your intended use is not permitted by statutory regulation or exceeds the permitted use, you will need to obtain permission directly from the copyright holder. To view a copy of this licence, visit http://creativecommons.org/licenses/by/4.0/.

References

1. O'Mahony AM, Silvester DS, Aldous L, Hardacre C, Compton RG (2008) Effect of water on the electrochemical window and potential limits of room-temperature ionic liquids. J Chem Eng Data 53:2884–2891
2. Yokoyama Y, Fukutsuka T, Miyazaki K, Abe T (2018) Origin of the electrochemical stability of aqueous concentrated electrolyte solutions. J Electrochem Soc 165:A3299–A3303
3. Baldelli S (2008) Surface structure at the ionic liquid-electrified metal interface. Acc Chem Res 41:421–431
4. Endres F (2002) Ionic liquids: solvents for the electrodeposition of metals and semiconductors. ChemPhysChem 3:144–154
5. Rogers RD, Seddon KR (2003) Ionic liquids-solvents of the future? Science 302:792–793
6. MacFarlane DR, Tachikawa N, Forsyth M, Pringle JM, Howlett PC, Elliott GD, Davis JH, Watanabe M, Simon P, Angell CA (2014) Energy applications of ionic liquids. Energy Environ Sci 7:232–250
7. Alwast D, Schnaidt J, Jusys Z, Behm RJ (2020) Ionic liquid electrolytes for metal-air batteries: interactions between O 2, Zn 2+ and H 2 O impurities. J Electrochem Soc 167:070505
8. Luo M, Koper MTM (2022) A kinetic descriptor for the electrolyte effect on the oxygen reduction kinetics on Pt(111). Nat Catal 5:615–623
9. Colic V, Pohl MD, Scieszka D, Bandarenka AS (2016) Influence of the electrolyte composition on the activity and selectivity of electrocatalytic centers. Catal Today 262:24–35
10. Zeledón JAZ, Kamat GA, Gunasooriya GTKK, Nørskov JK, Stevens MB, Jaramillo TF (2021) Probing the effects of acid electrolyte anions on electrocatalyst activity and selectivity for the oxygen reduction reaction. ChemElectroChem 8:2467–2478
11. Simeone FC, Kolb DM, Venkatachalam S, Jacob T (2007) The Au(111)/electrolyte interface: a tunnel-spectroscopic and DFT investigation. Angew Chem Int Ed 46:8903–8906
12. Bühlmeyer H, Hauner J, Eschenbacher R, Steffen J, Trzeciak S, Taccardi N, Görling A, Zahn D, Wasserscheid P, Libuda J (2023) Structure formation in an ionic liquid wetting layer: a combined STM, IRAS, DFT and MD Study of [C 2 C 1 Im][OTf] on Au(111). Chem A Eur J 29(46):e202301328
13. Maksymovych P, Sorescu DC, Yates JT (2006) Methanethiolate adsorption site on Au(111): a combined STM/DFT study at the single-molecule level. J Phys Chem B 110:21161–21167
14. Zhang Z, Wei Z, Sautet P, Alexandrova AN (2022) Hydrogen-induced restructuring of a Cu(100) electrode in electroreduction conditions. J Am Chem Soc 144:19284–19293
15. Kwon S, Kim Y-G, Baricuatro JH, Goddard WA (2021) Dramatic change in the step edges of the Cu(100) electrocatalyst upon exposure to CO: operando observations by electrochemical STM and explanation using quantum mechanical calculations. ACS Catal 11:12068–12074
16. Buchner F, Forster-Tonigold K, Uhl B, Alwast D, Wagner N, Farkhondeh H, Groß A, Behm RJ (2013) Toward the microscopic identification of anions and cations at the ionic liquid|Ag(111) interface: a combined experimental and theoretical investigation. ACS Nano 7:7773–7784
17. Andryushechkin BV, Shevlyuga VM, Pavlova TV, Zhidomirov GM, Eltsov KN (2018) STM and DFT Study of Chlorine Adsorption on the Ag(111)- p (44)–O Surface. The Journal of Physical Chemistry C 122:28862–28867
18. Kibler LA, Hermann JM, Matzik FM, Wittmann M, Fackler S, Jacob T (2024) In: Wandelt KK, Wandelt KK, (eds), *Surface preparation of well-defined electrodes: Single crystal electrochemistry*, Elsevier, pp 426–449
19. Atkin R, Borisenko N, Drüschler M, El Abedin SZ, Endres F, Hayes R, Huber B, Roling B (2011) An in situ STM/AFM and impedance spectroscopy study of the extremely pure 1-butyl-1-methylpyrrolidinium tris(pentafluoroethyl)trifluorophosphate/Au(111) interface: Potential dependent solvation layers and the herringbone reconstruction. Phys Chem Chem Phys 13:6849–6857
20. Borisenko N, El Abedin SZ, Endres F (2012) An in Situ STM and DTS study of the extremely pure [EMIM]FAP/Au(111) interface. ChemPhysChem 13:1736–1742
21. Howlett PC, Izgorodina EI, Forsyth M, MacFarlane DR (2006) Electrochemistry at negative potentials in bis(trifluoromethanesulfonyl) amide ionic liquids. Zeitschrift fur Physikalische Chemie 220:1483–1498
22. Kroon MC, Buijs W, Peters CJ, Witkamp G-J (2006) Decomposition of ionic liquids in electrochemical processing. Green Chem 8:241–245
23. Endres F, El Abedin SZ, Borissenko N (2006) Probing lithium and alumina impurities in air- and water stable ionic liquids by cyclic voltammetry and in situ scanning tunneling microscopy. Z Phys Chem 220:1377–1394

24. Randström S, Appetecchi G, Lagergren C, Moreno A, Passerini S (2007) The influence of air and its components on the cathodic stability of N-butyl-N-methylpyrrolidinium bis(trifluoromethanesulfonyl)imide. Electrochim Acta 53:1837–1842
25. Katayama Y, Onodera H, Yamagata M, Miura T (2004) Electrochemical reduction of oxygen in some hydrophobic room-temperature molten salt systems. J Electrochem Soc 151:A59
26. Randström S, Montanino M, Appetecchi GB, Lagergren C, Moreno A, Passerini S (2008) Effect of water and oxygen traces on the cathodic stability of N-alkyl-N-methylpyrrolidinium bis(trifluoromethanesulfonyl)imide. Electrochim Acta 53:6397–6401
27. Doblinger S, Donati TJ, Silvester DS (2020) Effect of humidity and impurities on the electrochemical window of ionic liquids and its implications for electroanalysis. J Phys Chem C 124:20309–20319
28. Hu X, Chen C, Tang S, Wang W, Yan J, Mao B (2015) An in situ STM investigation of EMITFSI ionic liquid on Au(111) in the presence of lithium salt. Sci Bull 60:877–883
29. Doblinger S, Lee J, Silvester DS (2019) Effect of ionic liquid structure on the oxygen reduction reaction under humidified conditions. J Phys Chem C 123:10727–10737
30. Schröder U, Wadhawan JD, Compton RG, Marken F, Suarez PAZ, Consorti CS, de Souza RF, Dupont J (2000) Water-induced accelerated ion diffusion: voltammetric studies in 1-methyl-3-[2,6-(S)-dimethylocten-2-yl]imidazolium tetrafluoroborate, 1-butyl-3-methylimidazolium tetrafluoroborate and hexafluorophosphate ionic liquids. New J Chem 24:1009–1015
31. Elkhafif OWAM, Hassan HK, Ceblin M, Farkas A, Jacob T (2023) Influence of residual water traces on the electrochemical performance of hydrophobic ionic liquids for magnesium-containing electrolytes. ChemSusChem 16(19):e202300421
32. Xu M, Ivey D, Xie Z, Qu W, Dy E (2013) The state of water in 1-butly-1-methyl-pyrrolidinium bis(trifluoromethanesulfonyl) imide and its effect on Zn/Zn(II) redox behavior. Electrochim Acta 97:289–295
33. Feng G, Jiang X, Qiao R, Kornyshev AA (2014) Water in ionic liquids at electrified interfaces: the anatomy of electrosorption. ACS Nano 8:11685–11694
34. Friedl J, Markovits IIE, Herpich M, Feng G, Kornyshev AA, Stimming U (2017) Interface between an Au(111) surface and an ionic liquid: the influence of water on the double-layer capacitance. ChemElectroChem 4:216–220
35. Bi S, Wang R, Liu S, Yan J, Mao B, Kornyshev AA, Feng G (2018) Minimizing the electrosorption of water from humid ionic liquids on electrodes. Nat Commun 9:5222
36. Huddleston JG, Visser AE, Reichert WM, Willauer HD, Broker GA, Rogers RD (2001) Characterization and comparison of hydrophilic and hydrophobic room temperature ionic liquids incorporating the imidazolium cation. Green Chem 3:156–164
37. Aldous L, Silvester DS, Villagrán C, Pitner WR, Compton RG, Cristina Lagunas M, Hardacre C (2006) Electrochemical studies of gold and chloride in ionic liquids. New J Chem 30:1576–1583
38. Motobayashi K, Shibamura Y, Ikeda K (2019) Potential-induced interfacial restructuring of a pyrrolidinium-based ionic liquid on an Au electrode: effect of polarization of constituent ions. Electrochem Commun 100:117–120
39. Schuett FM, Heubach M-K, Mayer J, Ceblin MU, Kibler LA, Jacob T (2021) Electrodeposition of Zinc onto Au(111) and Au(100) from the ionic liquid [MPPip][TFSI]. Angewandte Chemie 60:20461–20468
40. Appetecchi GB, Scaccia S, Tizzani C, Alessandrini F, Passerini S (2006) Synthesis of hydrophobic ionic liquids for electrochemical applications. J Electrochem Soc 153:A1685
41. Gnahm M, Kolb DM (2011) The purification of an ionic liquid. J Electroanal Chem 651:250–252
42. Sweeny BK, Peters DG (2001) Cyclic voltammetric study of the catalytic behavior of nickel(I) salen electrogenerated at a glassy carbon electrode in an ionic liquid (1-butyl-3-methylimidazolium tetrafluoroborate, BMIM+BF4-). Electrochem Commun 3:712–715
43. Breck DW (1964) Crystalline Molecular Sieves. J Chem Educ 41:678–689
44. Ntais S, Moschovi A, Paloukis F, Neophytides S, Burganos V, Dracopoulos V, Nikolakis V (2011) Preparation and ion transport properties of NaY zeolite–ionic liquid composites. J Power Sources 196:2202–2210
45. Atkin R, El Abedin SZ, Hayes R, Gasparotto LHS, Borisenko N, Endres F (2009) AFM and STM studies on the surface interaction of [BMP]TFSA and [EMIm]TFSA ionic liquids with Au(111). J Phys Chem C 113:13266–13272
46. Gasparotto LHS, Borisenko N, Bocchi N, Zein El Abedin S, Endres F (2009) In situ STM investigation of the lithium underpotential deposition on Au(111) in the air- and water-stable ionic liquid 1-butyl-1-methylpyrrolidinium bis(trifluoromethylsulfonyl) amide. Phys Chem Chem Phys 11:11140–11145
47. Rudnev AV, Ehrenburg MR, Molodkina EB, Abdelrahman A, Arenz M, Broekmann P, Jacob T (2020) Structural changes of Au(111) single-crystal electrode surface in ionic liquids. ChemElectroChem 7:501–508
48. Wen R, Rahn B, Magnussen OM (2015) Potential-dependent adlayer structure and dynamics at the ionic liquid/Au(111) interface: a molecular-scale in situ video-STM study. Angew Chem Int Ed 54:6062–6066
49. Berger CA, Ceblin MU, Jacob T (2017) Lithium deposition from a piperidinium-based ionic liquid: rapping dendrites on the knuckles. ChemElectroChem 4:261–265
50. Engstfeld AK, Hermann JM, Hörmann N, Rüth J (2023) svgdigitizer
51. Heubach M-K, Schuett FM, Kibler LA, Abdelrahman A, Jacob T (2022) Initial stages of sodium deposition onto Au(111) from [MPPip][TFSI]: an in-situ STM study for sodium-ion battery electrolytes. ChemElectroChem 9:e202200722
52. Schuett FM, Zeller SJ, Eckl MJ, Matzik FM, Heubach M, Geng T, Hermann JM, Uhl M, Kibler LA, Engstfeld AK, Jacob T (2021) Versatile 3D-printed micro-reference electrodes for Aqueous and non-Aqueous solutions. Angew Chem Int Ed 60:22783–22790
53. Villagrán C, Banks CE, Hardacre C, Compton RG (2004) Electroanalytical determination of trace chloride in room-temperature ionic liquids. Anal Chem 76:1998–2003
54. Seddon KR, Stark A, Torres M-J (2000) Influence of chloride, water, and organic solvents on the physical properties of ionic liquids. Pure Appl Chem 72:2275–2287
55. Barrosse-Antle LE, Bond AM, Compton RG, O'Mahony AM, Rogers EI, Silvester DS (2010) Voltammetry in room temperature ionic liquids: comparisons and contrasts with conventional electrochemical solvents. Chem Asian J 5:202–230
56. Silvester DS, Compton RG (2006) Electrochemistry in room temperature ionic liquids: a review and some possible applications. Zeitschrift fur Physikalische Chemie 220:1247–1274
57. Cuadrado-Prado S, Domínguez-Pérez M, Rilo E, García-Garabal S, Segade L, Franjo C, Cabeza O (2009) Experimental measurement of the hygroscopic grade on eight imidazolium based ionic liquids. Fluid Phase Equilib 278:36–40
58. Wasserscheid P, Welton T (eds) (2007) Ionic liquids in synthesis. Wiley, Hoboken
59. Heubach M-K, Bansmann J, Engstfeld AK, Jacob T (2024) Assessing the quality of ionic liquids using single crystal electrochemistry, surface science and data screening

60. Khan A, Zhao C (2015) Oxygen reduction reactions in aprotic ionic liquids based mixed electrolytes for high performance of Li–O_2 batteries. ACS Sustain. Chem. Eng 4(2):506–513. https://doi.org/10.1021/acssuschemeng.5b00890
61. Anthony JL, Anderson JL, Maginn EJ, Brennecke JF (2005) Anion effects on gas solubility in ionic liquids. J Phys Chem B 109(13):6366–6374. https://doi.org/10.1021/jp046404l
62. Nakamoto H, Suzuki Y, Shiotsuki T, Mizuno F, Higashi S, Takechi K, Asaoka T, Nishikoori H, Iba H (2013) Ether-functionalized ionic liquid electrolytes for lithium-air batteries. J Power Sources 243:19–23. https://doi.org/10.1016/j.jpowsour.2013.05.147
63. Hert DG, Anderson JL, Akia SNVK, Brennecke JF (2005) Enhancement of oxygen and methane solubility in 1-hexyl-3-methylimidazolium bis(trifluoromethylsulfonyl) imide using carbon dioxide. Chem Comm 20:2603–2605. https://doi.org/10.1039/B419157A
64. Zhang D, Okajima T, Matsumoto F, Ohsaka T (2004) Electroreduction of dioxygen in 1-n-Alkyl-3-methylimidazolium tetrafluoroborate room-temperature ionic liquids. J Electrochem Soc 151:D31
65. Yuan X-Z, Alzate V, Xie Z, Ivey DG, Qu W (2014) Oxygen reduction reaction in 1-Butyl-1-methyl-pyrrolidinium Bis(trifluoromethanesulfonyl)imide: addition of water as a proton species. J Electrochem Soc 161:A451–A457
66. Switzer EE, Zeller R, Chen Q, Sieradzki K, Buttry DA, Friesen C (2013) Oxygen reduction reaction in ionic liquids: the addition of protic species. J Phys Chem C 117:8683–8690
67. Aldous L, Silvester DS, Pitner WR, Compton RG, Lagunas MC, Hardacre C (2007) Voltammetric studies of gold, protons, and [HCl2]- in ionic liquids. J Phys Chem C 111:8496–8503

Publisher's Note Springer Nature remains neutral with regard to jurisdictional claims in published maps and institutional affiliations.